agriculture

MDPI

Article

Experimental Structural Safety Analysis of Front-End Loader of Agricultural Tractor

Jeong-Hun Kim [1,2,†], Dong-Hyeon Gim [3,†] and Ju-Seok Nam [1,2,*]

[1] Department of Biosystems Engineering, College of Agriculture and Life Sciences, Kangwon National University, Chuncheon 24341, Gangwon-do, Republic of Korea; jhkim1995@kangwon.ac.kr
[2] Interdisciplinary Program in Smart Agriculture, Kangwon National University, 1 Kangwondaehak-gil, Chuncheon 24341, Gangwon-do, Republic of Korea
[3] CAE Solution Department of TYMICT, Gongju 32530, Chungcheongnam-do, Republic of Korea; dhkim9075@tymict.com
* Correspondence: njsg1218@kangwon.ac.kr; Tel.:+82-33-250-6497
† These authors contributed equally to this work.

Abstract: The agricultural front-end loader is an implement attached to the front of tractors to transport various agricultural materials, including soil. Since they are subjected to various loads due to the working environment, their safety analysis in consideration of actual working conditions is required. However, there are no official standardized test codes to consider various actual working environments currently. In this study, the structural safety of a front-end loader for static and fatigue failures was evaluated using new test code reflecting actual working environments. Thirty-four measurement locations were determined as the stress concentration spots of each component of the front-end loader derived through multibody dynamic simulation. The total testing time was set to 1 h, and the test time for each task was determined considering the duty percentage of the actual loader work. The measurement results showed that the maximum stress that exceeds the material's yield strength occurred at two locations of the mount, which is the connection to the tractor body, resulting in static yielding. For tasks, the pulling and dumping exhibited the highest stress. The task that had the largest impact on fatigue damage was the dumping. The static safety factor was found to be over 1.93 and the fatigue life met the required lifespan at all measurement locations except for those exhibiting static yielding. Therefore, the most vulnerable part of the front-end loader is the mount, and it is necessary to secure the overall structural integrity by robust design for the mount.

Keywords: failure; fatigue life; front-end loader; static safety factor; structural safety

check for updates

Citation: Kim, J.-H.; Gim, D.-H.; Nam, J.-S. Experimental Structural Safety Analysis of Front-End Loader of Agricultural Tractor. *Agriculture* **2024**, *14*, 947. https://doi.org/10.3390/agriculture14060947

Academic Editors: Chung-Liang Chang and Mustafa Ucgul

Received: 16 May 2024
Revised: 13 June 2024
Accepted: 15 June 2024
Published: 18 June 2024

Copyright: © 2024 by the authors. Licensee MDPI, Basel, Switzerland. This article is an open access article distributed under the terms and conditions of the Creative Commons Attribution (CC BY) license (https://creativecommons.org/licenses/by/4.0/).

1. Introduction

Various implements have been mounted on prime movers to improve the efficiency and productivity of agricultural work [1]. Among them, the front-end loader is attached to the front of the agricultural tractors and controlled through tractor hydraulic systems to transport soil, agricultural products, and byproducts [2,3]. The front-end loader can fail or become deformed under large loads when it performs loading or unloading and is exposed to irregular road surfaces or obstacles due to the nature of the working environment [4,5]. Such failure and deformation significantly affect the productivity and work efficiency as well as the safety of workers [6,7]. Therefore, the front-end loader needs to be designed to have a safe structure and its safety must be verified through tests [8,9].

Only a few studies have been conducted on the agricultural front-end loader. Cho et al. analyzed the impact reduction effect of the boom suspension through hydraulic simulation to reduce the vibration and impact generated by the bumps on the ground. They improved the hydraulic system of the front-end loader based on simulation results and verified the impact reduction effect by performing an actual vehicle test [10]. Ahn et al. conducted research for reducing the vibration and impact from the front-end loader using

an accumulator [11]. Latoree et al. developed an automatic leveling system by controlling the posture of the front-end loader during work on slopes or irregular surfaces. They expected this to reduce the labor of farmers and improve their productivity [12]. Kwon and Shin conducted structural analysis by using the load derived through hydraulic system analysis and evaluated the structural safety of the front-end loader. They also performed design optimization based on the structural analysis results [13]. In addition to structural analysis, studies evaluating the safety of front-end loaders based on measurements have also been conducted. In these studies, most instrumentation systems use strain gauges to reduce costs and enable miniaturization [14]. Malon et al. measured the stress of front-end loader components under static and dynamic loadings to the bucket for the development of a structural analysis model of the front-end loader. They verified the accuracy of the model by comparing the stress measurements with the structural analysis results [15]. Park et al. evaluated the structural safety of a front-end loader by measuring the stress generated during the drop and impact tests for the bucket [16]. Thus far, the structural safety of front-end loaders mainly considered the effects of static or dynamic loads from the weight on the bucket, as well as simple operations with a few impact conditions. However, when using a front-end loader for various tasks, diverse loads can occur in various working environments. There are no official standardized test codes to consider these various working conditions, and front-end loader manufacturers have tested their product by considering some simple impact conditions. Therefore, it is necessary to develop a test code to reflect various working conditions and evaluate the front-end loader safety based on the test code.

In this study, we suggest new test code for the front-end loader considering the actual working environments, and evaluate the structural safety based on the measurement following the code. The following conditions were included in the test code: the occurrence of static and dynamic loads caused by the payload of bucket, the occurrence of an impact load due to an obstacle, traveling on an irregular road surface with bumps, and the operation of loading, transportation, and unloading of soil. Based on the stress measurement results, the vulnerable part of the front-end loader was identified. The results of this study are expected to be used as foundational data for front-end loader design and verification.

2. Materials and Methods

2.1. Tractor and Front-End Loader

In this study, tests were conducted by attaching a front-end loader to an 18 kW-class agricultural tractor (TYM, Gongju, Korea). The tractor used for the tests weighs 8.19 kN, with a wheelbase of 1670 mm and a ground clearance of 240 mm. The front-end loader used is a product of the parallel link type with two boom cylinders and two bucket cylinders. The front-end loader weighs 4.5 kN, and the capacity and maximum allowable payload of the bucket are 0.23 m^3 and 5.96 kN, respectively. Tables 1 and 2 list the specifications of the tractor and the front-end loader, respectively. Figure 1 shows the shape of the tractor and the front-end loader. The frame of the front-end loader consists of a bucket, booms, posts, and mounts and rear frames for connecting to a tractor. The characteristics of each component are as follows:

Table 1. Specification of the tractor used.

Item	Specification
Model/Company/City/Nation	T2515/TYM/Gongju/Korea
Engine rated power (kW)	18
Engine rated speed (rpm)	2100
Total weight (kN)	8.19
Overall length × width × height (mm)	2395 × 1170 × 2500
Wheelbase (mm)	1670
Ground clearance (mm)	240

Table 2. Specifications of the front-end loader used.

Item	Specification
Model/Company/City/Nation	BL150/TYM/Gongju/Korea
Bucket capacity (m^3)	0.23
Total weight (kN)	4.5
Maximum lift height (mm)	2665
Maximum allowable payload (kN)	5.96

Figure 1. View of the tractor and front-end loader used: (**a**) tractor; (**b**) front-end loader; (**c**) front-end loader attached to the tractor.

A. Bucket: It is the loading part that directly loads soil, agricultural products, and byproducts, and its movement is controlled by bucket cylinders.

B. Boom: It is the main frame of the front-end loader equipped with the bucket at the end, and its movement is controlled using boom cylinders.

C. Post: It is the connecting frame of the boom, boom cylinder, and mount. It supports the reaction force generated by the operation of boom cylinders.

D. Mount: It connects the post to the tractor body. It is fastened to the bottom of the engine room of the tractor to support the weight of the loader and the impact and vibration generated during operation.

E. Rear frame: It connects the mount to the rear axle of the tractor to share the impact and vibration from the mount.

2.2. Test Condition

The test conditions were determined based on a newly proposed test code by the front-end loader manufacturer. They included five tasks: drop test, impact test, pulling test, driving test, and dumping test. The drop test considers the case where the load is generated by the payload when the bucket of the front-end loader rises and falls. The impact and pulling tests consider cases where an impact occurs due to an obstacle or an excessive payload is applied to the bucket. The driving test considers the vibration caused by the irregular road surface while traveling, and the dumping test considers the work of loading, transportation, and unloading of soil. In all test conditions, a rear ballast load of 3.0 kN was applied for safe operation. The drop, impact, and driving tests were conducted by applying a payload of 2.5 kN to the bucket and a ballast weight of 3.0 kN to the rear of the tractor. In the pulling and dumping tests, only a rear ballast weight of 3.0 kN was applied with no payload on the bucket. Figure 2 shows the photographs of the tests. All the tests were conducted by skilled workers. The steps performed for the different tests were as follows:

A. Drop test: The bucket was first lifted to a maximum height of 2665 mm and then dropped until its bottom reached a height of 300 mm from the ground. In this instance, the boom cylinder was controlled so that the boom could move at maximum speed.

B. Impact test: The left and right ends of the bucket collided with the upper and lower parts of the impact test structure at a traveling speed of 1 km/h. The structure was made of steel and was fixed using anchors to prevent shaking at the time of the impact.

C. Pulling test: After fixing the left and right end, and the center of the bucket to the ground using a 300 mm long chain, the bucket was lifted repeatedly. In this case, the boom cylinder was controlled so that the boom could operate at maximum speed.

D. Driving test: The tractor was driven at a speed of 1 km/h on a circular paved road equipped with various bumps provided by the manufacturer.

E. Dumping test: Loading was performed to fill the bucket with soil, following which a straight-line distance of 20 m was traveled, and, subsequently, unloading was performed. When the transport of the piled soil was completed, the tractor was driven backwards with the bottom of the bucket touching the ground to level the soil.

The total testing time was set to 1 h, and the testing time for each test condition was determined considering the duty percentage. The driving and dumping tests were continuous tests, whereas the drop, impact, and pulling tests were discontinuous tests. For the latter, the number of tests was determined considering the testing time to be performed and the time required for one test. Table 3 shows the duty percentage provided by the manufacturer and the testing time for each condition based on 1 h of total time.

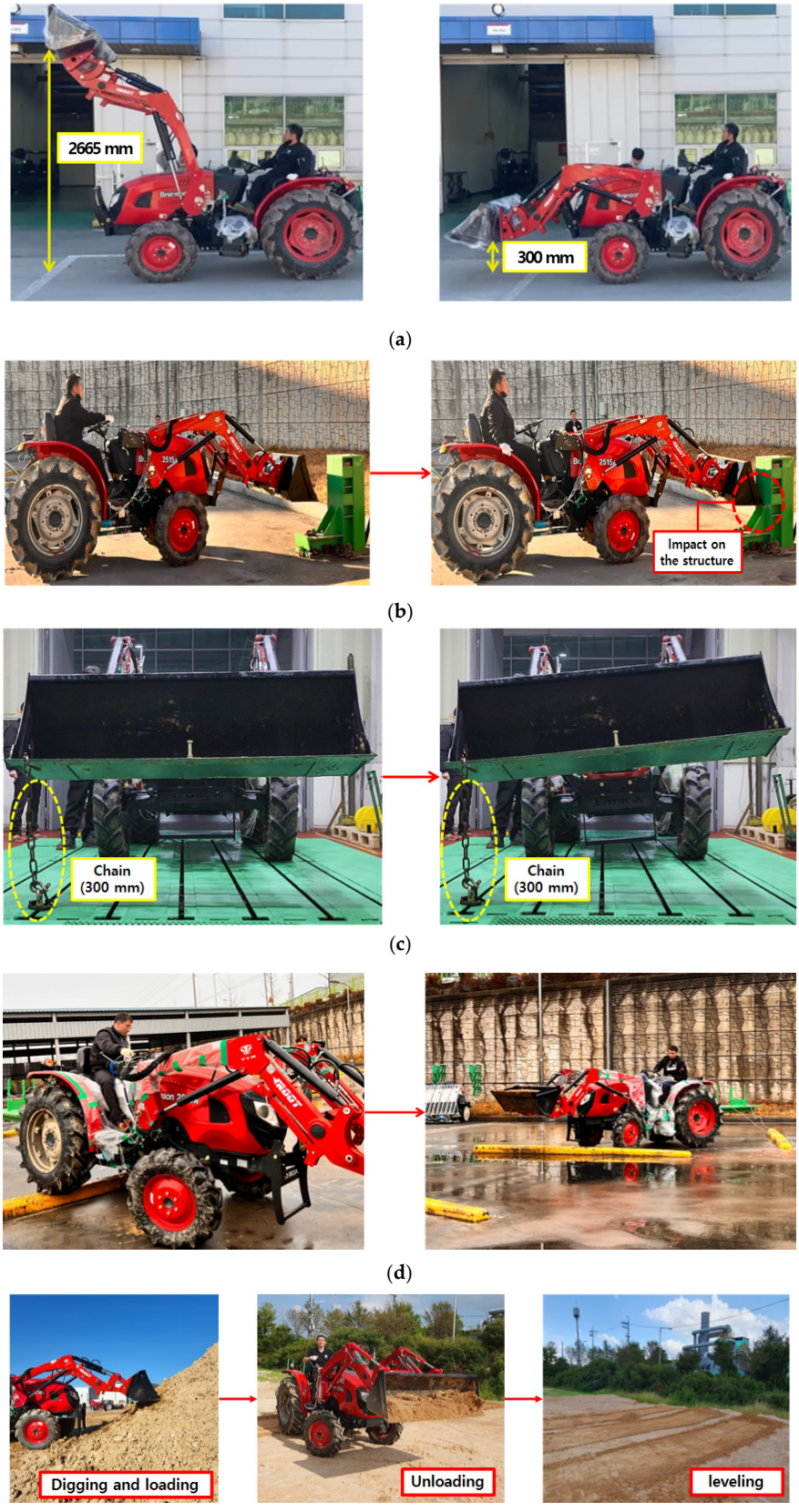

Figure 2. Test conditions of the front-end loader: (**a**) drop test; (**b**) impact test; (**c**) pulling test; (**d**) driving test; (**e**) dumping test.

Table 3. Duty percentage and test time for each test.

Test Type		Duty Percentage (%)	Test Time (s)
Drop test		3.4	122.4
Impact test	Left-end of bucket to lower part of structure	1.0	7.2
	Left-end of bucket to upper part of structure		10.8
	Right-end of bucket to lower part of structure		10.8
	Right-end of bucket to upper part of structure		7.2
Pulling test	Chain on center of bucket	2.8	33.6
	Chain on left-end of bucket		33.6
	Chain on right-end of bucket		33.6
Driving test		46.4	1670.4
Dumping test		46.4	1670.4
Total		100	3600

2.3. Stress Measurement

2.3.1. Determination of the Stress Concentration Spots in the Front-End Loader

The stress concentration spots of the front-end loader components and the principal stress directions there were analyzed using commercial multibody dynamic analysis software (Recurdyn V9R5, Functionbay, Seongnam, Korea). Figure 3 shows the 3D model of the front-end loader used in the dynamic simulation. The 3D model was developed by reflecting the actual geometry and material properties of the front-end loader. The weight difference between the 3D model and the actual front-end loader was approximately 1%, indicating that the developed 3D model was valid (Table 4).

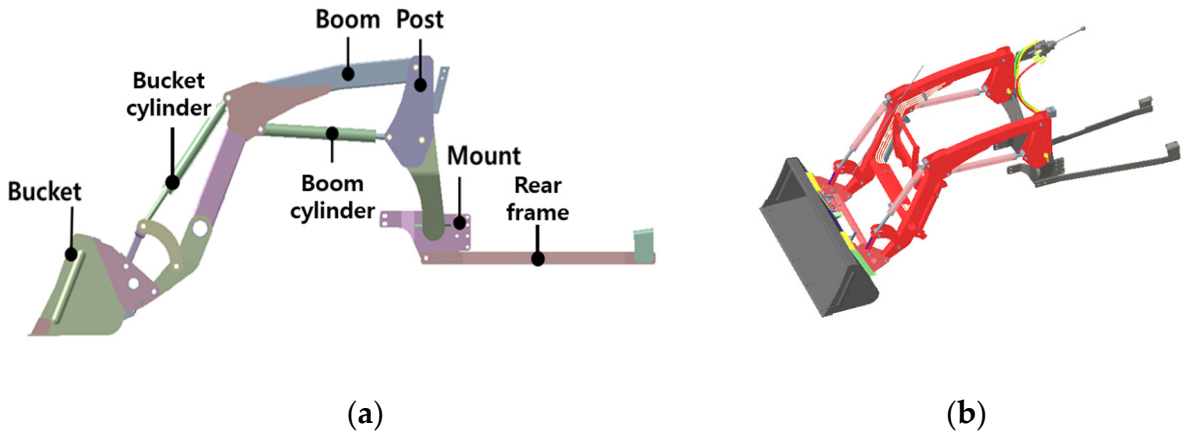

Figure 3. 3D model of the front-end loader: (**a**) side view; (**b**) ISO metric view.

Dynamic simulation was performed for the drop, pulling, and impact tests in which the occurrence of large instantaneous loads was expected. Figure 4 shows the simulation models created for each test condition. For the simulation of the drop test, a maximum allowable payload of 5.96 kN was added to the bucket and reciprocating lifting and dropping motion was applied within a height from 300 mm to 2655 mm as the actual test. The actuating force of the boom cylinder for moving the boom at maximum speed was determined to be 24.03 kN by an experiment. In the impact test simulation, a rigid body was created as an impact structure and this structure was allowed to hit the bucket at a speed of 1 km/h. In this case, a payload of 5.96 kN was applied to the bucket. In the

pulling test simulation, the bucket was located at a height of 300 mm from the rigid ground. While the ground and the bucket were connected using a rigid chain, the boom was raised at maximum speed. In all simulations, the mount and rear frame were fixed with a fixed support constraint. In the simulations of the drop and impact tests, the maximum allowable payload was applied to the bucket, unlike the actual test conditions, to clearly reveal stress concentration spots by the loads.

Table 4. Weight of the 3D model and actual front-end loader.

Item	Weight (kN)	
	3D Model	Actual Product
Bucket	1.27	4.5
Link	0.14	
Boom cylinder	0.22	
Boom	0.90	
Bucket cylinder	0.20	
Post	0.30	
Mount	0.92	
Rear frame	0.50	
Total	4.45	4.5

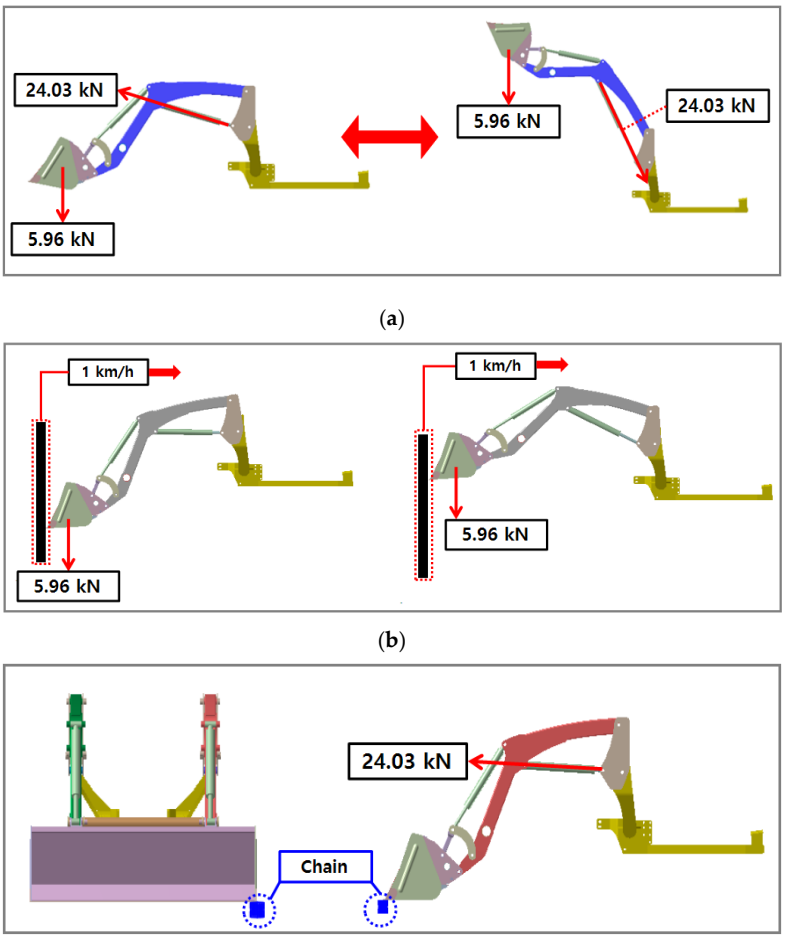

Figure 4. Multibody dynamic simulation models of the front-end loader: (**a**) drop test; (**b**) impact test; (**c**) pulling test.

The stress levels of the boom, post, mount, and rear frame, which are load-bearing frames among the components of the front-end loader and whose design can be changed relatively easily, were obtained from simulations. To facilitate analysis and save time, only the boom, post, mount, and rear frame were set as flexible bodies, while the other elements were constructed to rigid bodies. A square-shaped mesh was chosen for the flexible body analysis and its size ranged from 10 to 14.5 mm depending on the location. In the simulation results, a total of 34 stress concentration spots were derived with the principal stress directions, including 12 for the boom, 6 for the post, 8 for the mount, and 8 for the rear frame (Figure 5 and Table 5). In Figure 5, higher stress levels are represented in red, while lower stress levels are represented in blue. Since the front-end loader used in this study was horizontally symmetrical, the left side was marked with L and the right side with R based on the traveling direction of the tractor (Table 5).

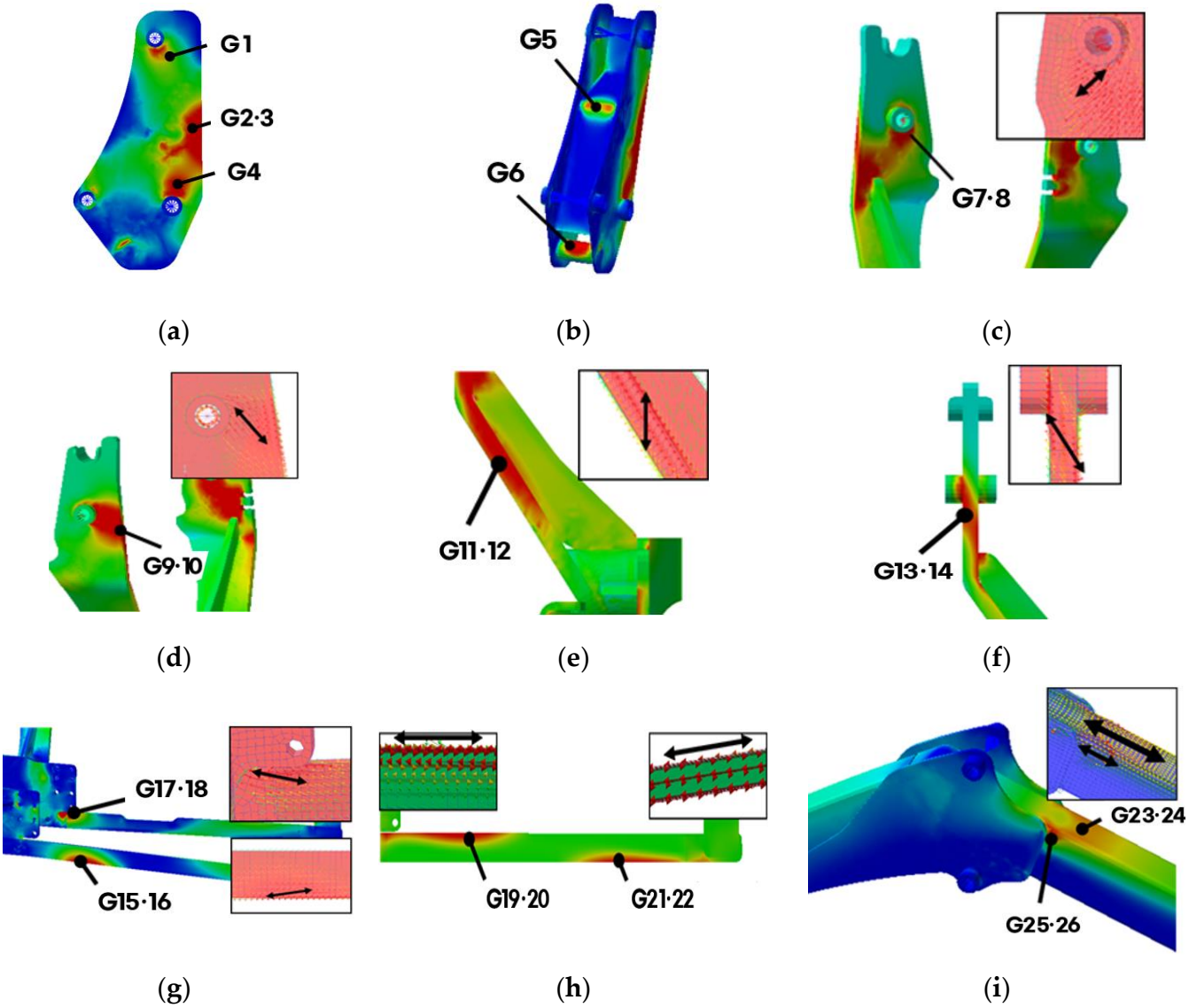

Figure 5. *Cont.*

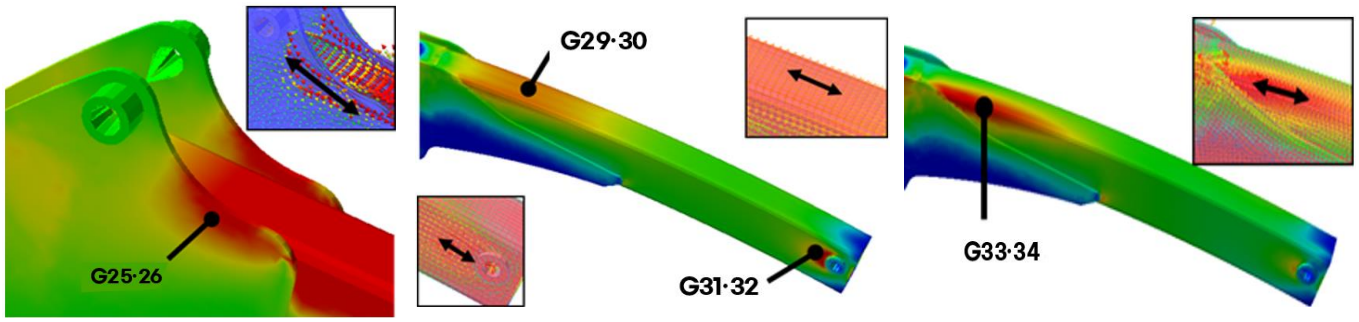

(**j**) (**k**) (**l**)

Figure 5. Stress of the front-end loader components from dynamic simulation: (**a**) post rear side; (**b**) post inside; (**c**) mount inside; (**d**) mount outside; (**e**) mount upper back side; (**f**) mount lower back side; (**g**) rear frame outside and upper inside; (**h**) rear frame upper and bottom side; (**i**) boom front top and inside; (**j**) boom side plate; (**k**) boom rear top and inside; (**l**) boom rear inside.

Table 5. Result of stress concentration location of each front-loader component through dynamic simulation.

Component	Symbol	Location	Component	Symbol	Location
Post	G1	Post upper collar	Rear frame	G18	Rear frame inside (R)
	G2	Post back side (L)		G19	Rear frame outside upper (L)
	G3	Post upper collar (R)		G20	Rear frame outside upper (R)
	G4	Post lower collar		G21	Rear frame rear bottom (L)
	G5	Post plate		G22	Rear frame rear bottom (R)
	G6	Post bar	Boom	G23	Front boom top side (L)
Mount	G7	Mount collar inside (L)		G24	Front boom top side (R)
	G8	Mount collar inside (R)		G25	Front boom inside (L)
	G9	Mount collar outside (L)		G26	Front boom inside (R)
	G10	Mount collar outside (R)		G27	Boom side plate (L)
	G11	Mount back side lower (L)		G28	Boom side plate (R)
	G12	Mount back side lower (R)		G29	Rear boom top side (L)
	G13	Mount back side upper (L)		G30	Rear boom top side (R)
	G14	Mount back side upper (R)		G31	Rear boom collar (L)
Rear frame	G15	Rear frame outside lower (L)		G32	Rear boom collar (R)
	G16	Rear frame outside lower (R)		G33	Rear boom inside (L)
	G17	Rear frame inside (L)		G34	Rear boom inside (R)

2.3.2. Measurement System

Uniaxial strain gauges were attached to the 34 stress concentration spots, determined from the dynamic simulation, in the principal stress direction (Figure 6). The strain gauges were connected to a bridge box (CANHEAD) and the data were transmitted to a data acquisition (DAQ) system via controller area network (CAN) communication. The data collected in the DAQ system were checked and stored in real time through a laptop. Figure 7 shows the outline of the measurement system and Table 6 lists the specifications of the strain gauge and bridge box. The strain measured using the strain gauge was converted into stress using Equation (1).

$$\sigma = E \times \varepsilon \quad (1)$$

where σ is the measured normal stress, MPa; E is modulus of elasticity, MPa; ε is measured normal strain, mm/mm.

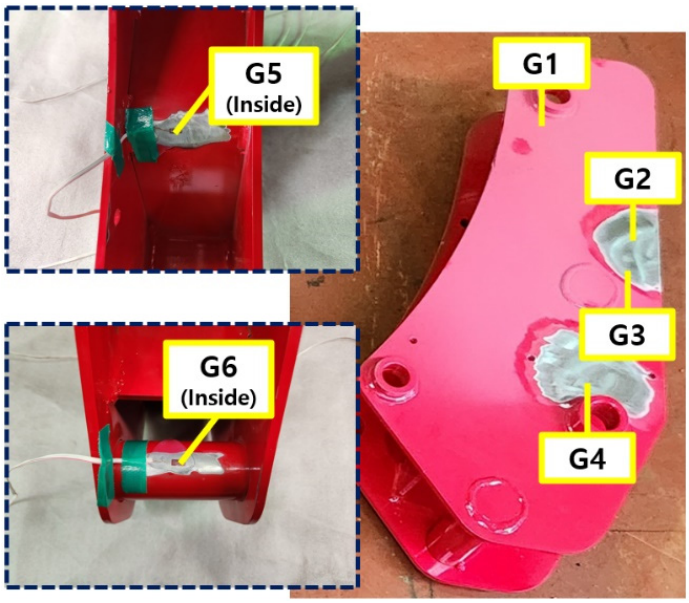

(a)

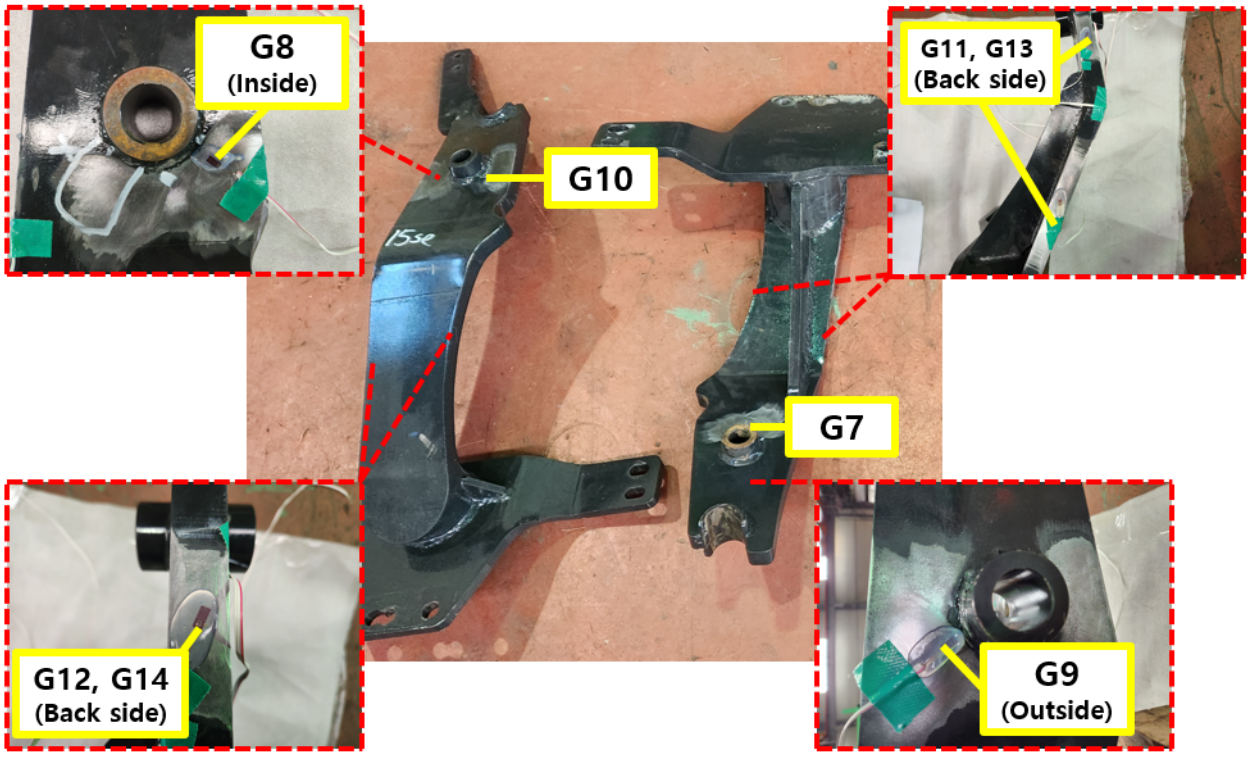

(b)

Figure 6. *Cont.*

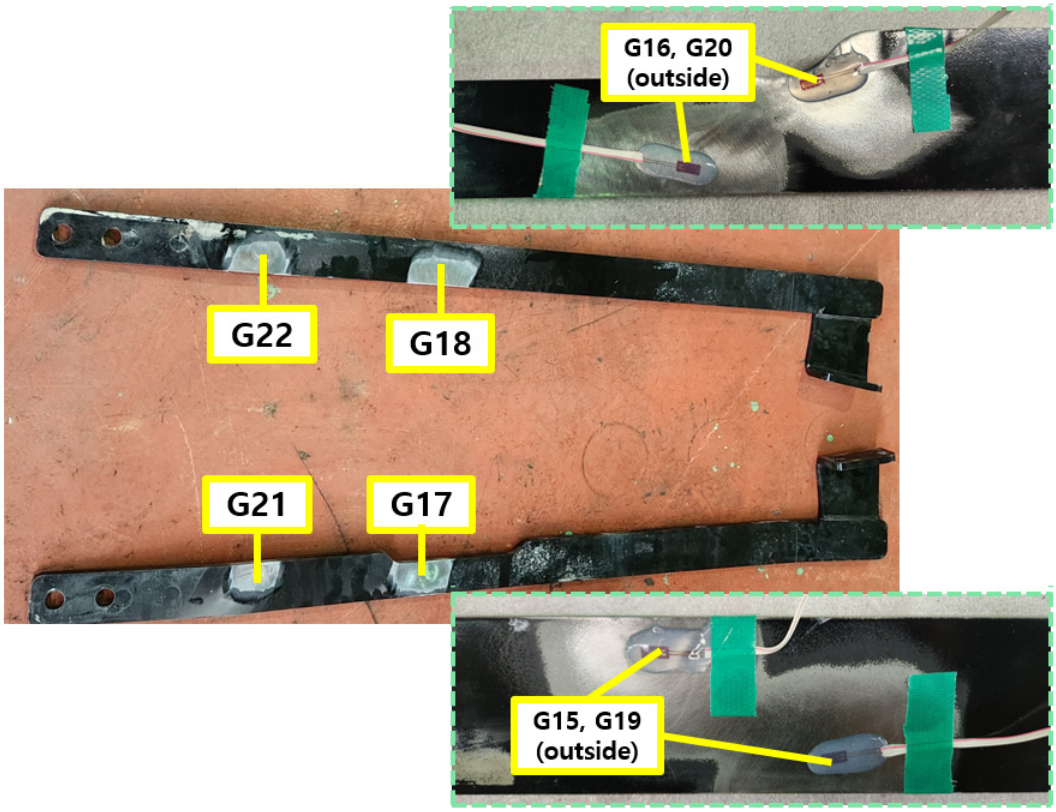

(**c**)

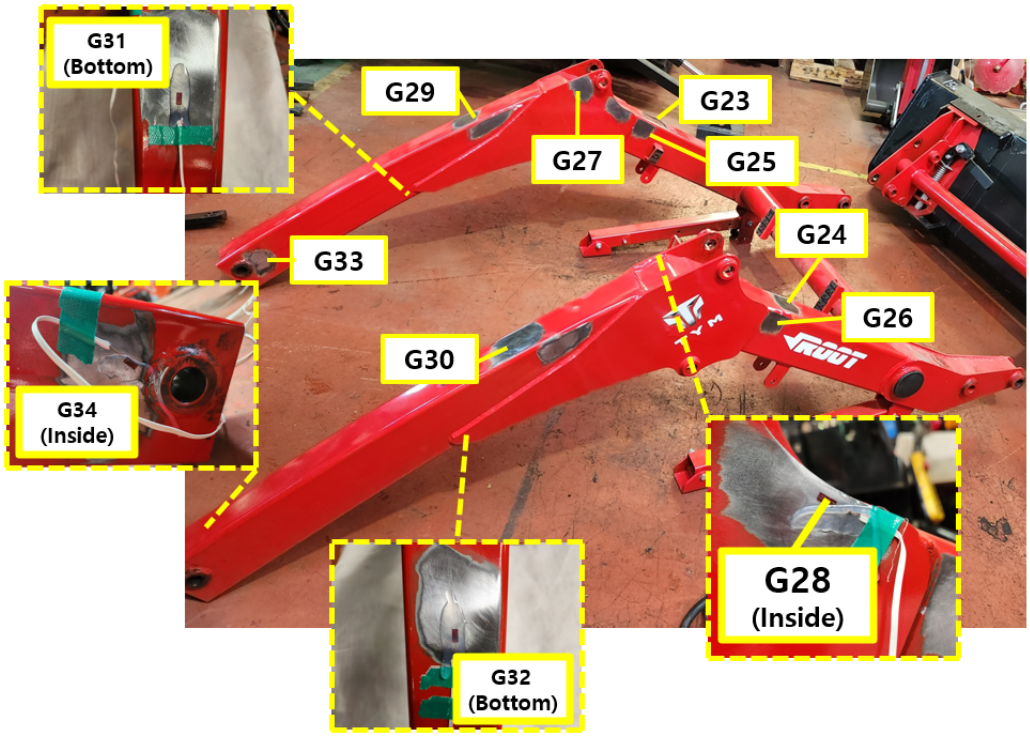

(**d**)

Figure 6. Attachment location of strain gauges: (**a**) post; (**b**) mount; (**c**) rear frame; (**d**) boom.

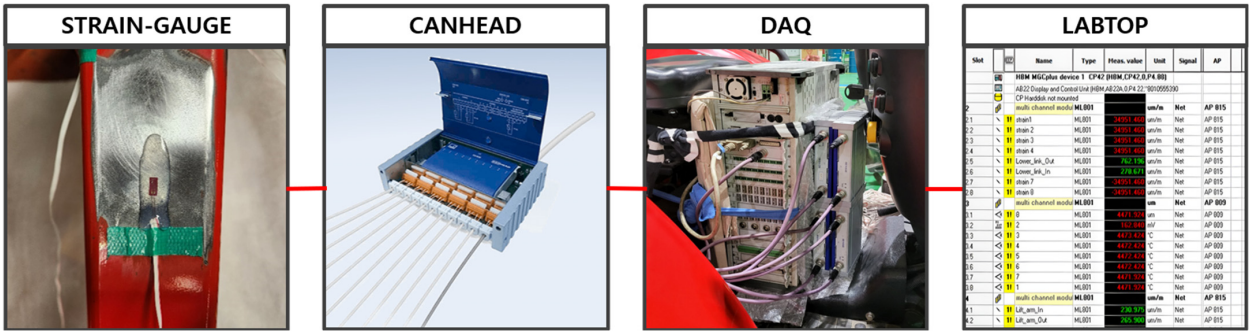

Figure 7. Diagram of the stress measurement system.

Table 6. Specification of the strain gauge and bridge box.

Item		Value
Strain gauge	Model/Company/City/Nation	KFGS−5−350−C1−11 /KYOWA/Tokyo/Japan
	Gauge factor	2.14 ± 1.0%
	Gauge length (mm)	5
	Gauge resistance (Ω)	350.0 ± 2.4
Bride box	Model/Company/City/Nation	CANHEAD/HBK/Seongnam/Korea
	Bridge excitation voltage (V)	2.5
	Measuring ranged (mV/V)	4
	Maximum sampling rate (kHz)	300
	Applicable temperature range (°C)	−30~70

2.4. Safety Analysis

2.4.1. Static Safety Factor

The static safety factor is an indicator of how safely agricultural machinery can respond to instantaneous high loads during agricultural work [17]. It is used to evaluate and improve the safety of the agricultural machinery in the design stage considering the strength of the materials and the working environment. The stress-based static safety factor is defined as the ratio of the allowable strength of the material to the maximum stress acting on it. If the static safety factor is higher than 1.0, the material can be judged to be safe for static loads. However, if it is less than 1.0, static failure can occur to the part or the structure [18]. In this study, the static safety factor was calculated using Equation (2) and the static safety of the front-end loader components was analyzed.

$$\text{S.F.} = \left| \frac{S_y}{\sigma_{max}} \right| \quad (2)$$

where S.F. is static safety factor, S_y is tensile yield strength of the material, MPa, and σ_{max} is measured maximum normal stress during the operation, MPa.

2.4.2. Fatigue Life

Failure to the mechanical parts and structures can occur due to the fatigue caused by repeated small loads as well as the high stress that exceeds the yield strength of the material [19,20]. Since the front-end loader is subjected to repeated loads while performing various tasks, safety against fatigue failure must also be evaluated.

The stress data measured in the time domain by the strain gauge were converted into the stress data in the frequency domain using the rain-flow counting method, thus making it possible to obtain the mean stress, the stress amplitude, and the frequency of that stress occurring [21]. The stress with the mean and amplitude were converted into the equivalent

completely reversed stress with a mean of zero using the Goodman's equation given in Equation (3).

$$\sigma_{eq} = \frac{S_u \times \sigma_a}{S_u - \sigma_m} \quad (3)$$

where σ_{eq} is equivalent completely reserved stress, MPa; S_u is ultimate tensile strength of the material, MPa; σ_a is measured stress amplitude, MPa; σ_m is measured mean stress, MPa.

It is possible to obtain the fatigue life cycle by applying the derived equivalent completely reversed stress to the stress–life (S–N) curve of the material. Fatigue damage was calculated using the actual frequency of the stress from rain-flow counting and the life cycle from S–N curve, by the Palmgren–Miner's linear cumulative damage rule, as shown in Equation (4).

$$D_t = \sum_{i=1}^{k} \frac{n_i}{N_i} \quad (4)$$

where D_t is total damage sum, n_i is number of actually applied cycles for the ith stress, and N_i is life cycles for ith stress.

The linear cumulative damage rule provides the total damage sum by adding the partial damage caused by all applied loads under the assumption that fatigue damage was linearly accumulated. It assumes that the fatigue failure of the material occurs when the total damage sum becomes 1.0 [22]. The fatigue life based on the total damage sum was calculated using Equation (5):

$$L_f = \frac{1}{D_t} \times t \quad (5)$$

where L_f is fatigue life and t is working time which generate damage sum.

In this study, commercial fatigue analysis software (nCode 2022, HBM Prenscia, Detroit, MI, USA) was used to calculate the fatigue damage and fatigue life. The calculation process was constructed by applying rain-flow counting, Goodman's equation, and Palmgren–Miner's linear cumulative damage rule to the measured time-domain stress data (Figure 8).

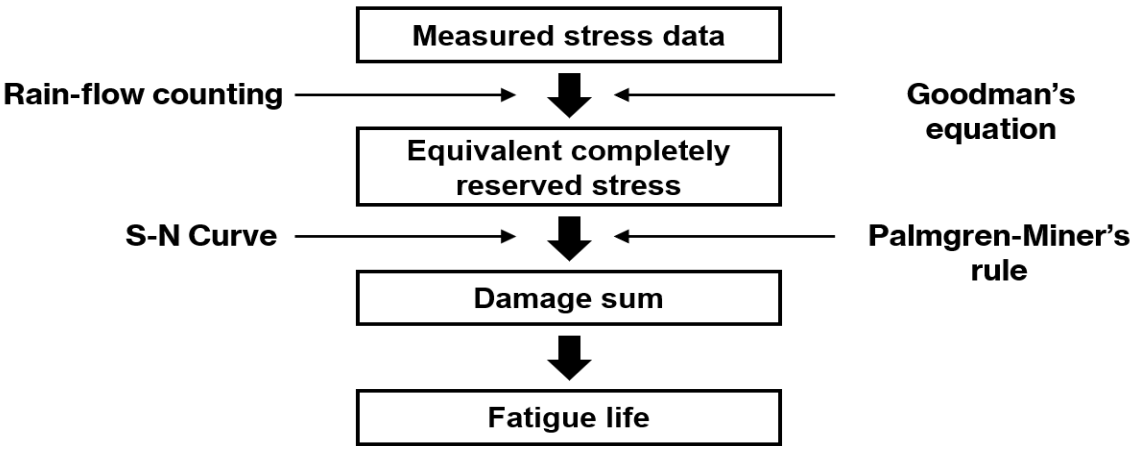

Figure 8. Process diagram to calculate the fatigue life.

The boom, post, mount, and rear frame of the front-end loader were made of the same material, and the S–N curve was obtained by reflecting the actual properties of the material (Figure 9 and Table 7). The components of the front-end loader are made from the same material, simplifying the manufacturing process, and reducing costs.

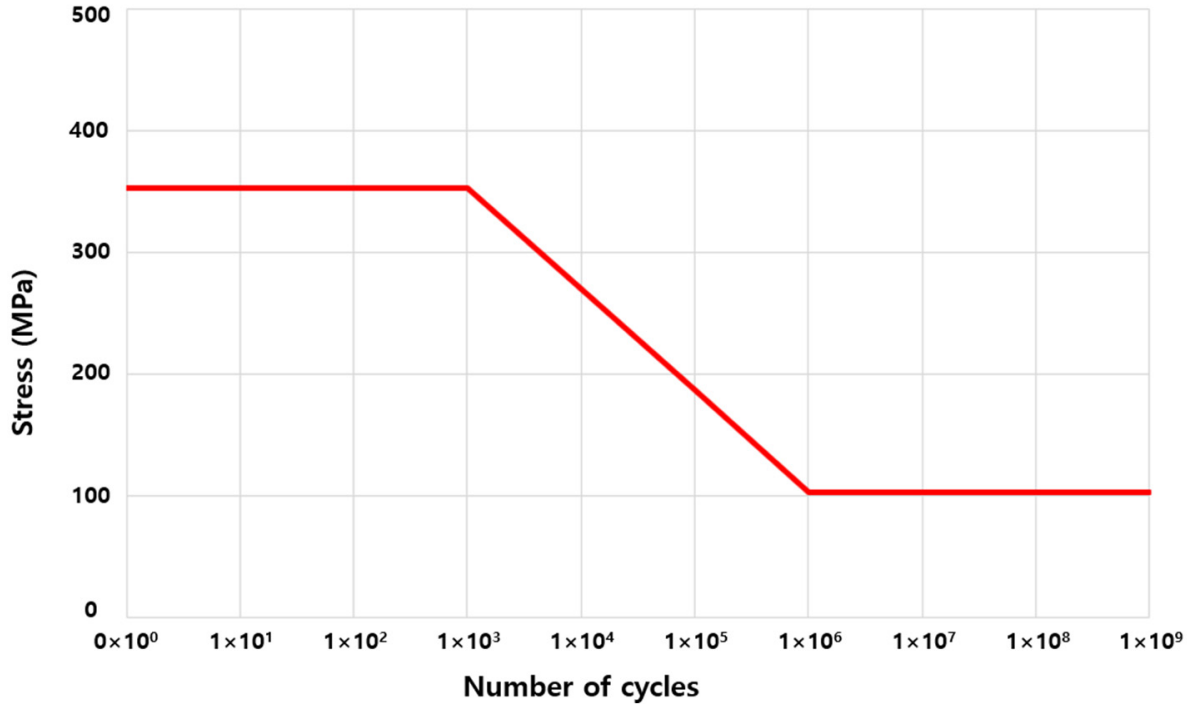

Figure 9. S–N curve of the front-end loader components.

Table 7. Material properties of the front-end loader components.

Item	Material Properties
Material	SS400
Tensile yield strength (MPa)	331
Ultimate tensile strength (MPa)	472
Elastic modulus (GPa)	202

3. Results and Discussion

3.1. Stress Measurement Results

The shape of the total measurement data at the gauge G1 considering the duty percentage by the test condition is shown in Figure 10. The stress trend was similar at all locations. In the drop test, the stress tended to increase when the bucket ascended compared to when it descended. In the impact test, lower stress occurred compared to the drop test. This indicates that a larger amount of damage occurs to the front-end loader when it rapidly raises and lowers the bucket compared to when it collides with obstacles at a speed of 1 km/h. The average stress during the driving test ranged from 5 to 60 MPa, depending on the measurement location, which was found to be the level that has no significant impact on the front-end loader damage. The maximum stress ranged from 28.86 to 3015 MPa depending on the measurement location, and it occurred in the pulling or dumping test (Table 8). In the pulling test, when the bucket was raised, the front-end loader acted as a cantilever due to the chain fixed to the ground. This appears to have caused a large stress on the components due to bending. In addition, it is thought that a large stress occurred in the dumping test because large bending loads were applied to the front-end loader by the payload while performing loading and unloading.

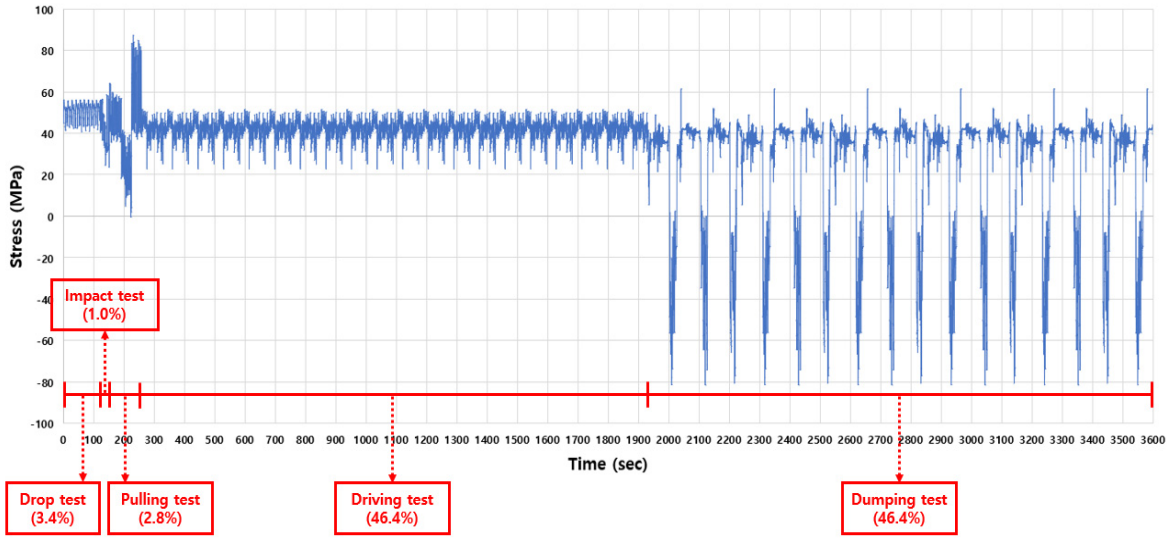

Figure 10. Shape of measure time-domain stresses at the gauge G1.

Table 8. Maximum stresses for each measurement location.

Component	Location	Maximum Stress (MPa)	Test Condition	Component	Location	Maximum Stress (MPa)	Test Condition
Post	G1	87.36	Pulling test	Rear frame	G18	36.42	Dumping test
	G2	−68.13	Dumping test		G19	−60.22	Pulling test
	G3	126.50	Dumping test		G20	−37.60	Pulling test
	G4	−116.20	Dumping test		G21	−171.70	Dumping test
	G5	−29.97	Dumping test		G22	−129.70	Dumping test
	G6	157.90	Dumping test	Boom	G23	83.26	Pulling test
Mount	G7	35.28	Dumping test		G24	96.83	Dumping test
	G8	−80.26	Pulling test		G25	95.68	Pulling test
	G9	68.00	Pulling test		G26	85.46	Pulling test
	G10	−54.57	Dumping test		G27	46.69	Pulling test
	G11	581.50	Pulling test		G28	47.50	Dumping test
	G12	−3015	Dumping test		G29	133.10	Dumping test
	G13	92.47	Pulling test		G30	112.00	Dumping test
	G14	106.60	Pulling test		G31	−81.01	Pulling test
Rear frame	G15	58.91	Dumping test		G32	−53.62	Dumping test
	G16	38.78	Pulling test		G33	63.31	Dumping test
	G17	28.86	Pulling test		G34	46.12	Pulling test

At the G12 and G11 locations of the mount, maximum stresses of 3015 and 581.5 MPa that exceeded the yield strength of the material occurred in the dumping and pulling tests, respectively. They were followed by maximum stresses of 171.70 and 157.90 MPa at the G21 location of the rear frame (dumping test) and the G6 location of the post (dumping test), respectively (Figure 11). The mount is a fastening element that fixes the front-end loader to the tractor body. It is the element to which the weight and working load of the front-end loader is first transferred. In particular, the G11 and G12 locations of the mount were located in the middle of the post–mount joint and mount–tractor body joint. Therefore, it appears that the application of an external load while both ends were fixed acted as a large bending load at the G11 and G12 locations, resulting in the maximum stress that exceeded the yield strength of the material. Relatively large stress also occurred at the G6 location of the post and the G21 location of the rear frame, even though it was lower than the yield strength of the material. It is believed that high stress occurred at the G6 location of the post because it was located in the transfer path of the load of the front-end loader at the post–mount joint. In addition, the G21 location of the rear frame was close to the mount–rear frame joint, and it was inferred that a high stress occurred

because it was located in the path where the load of the mount was transferred to the rear frame (Figure 12).

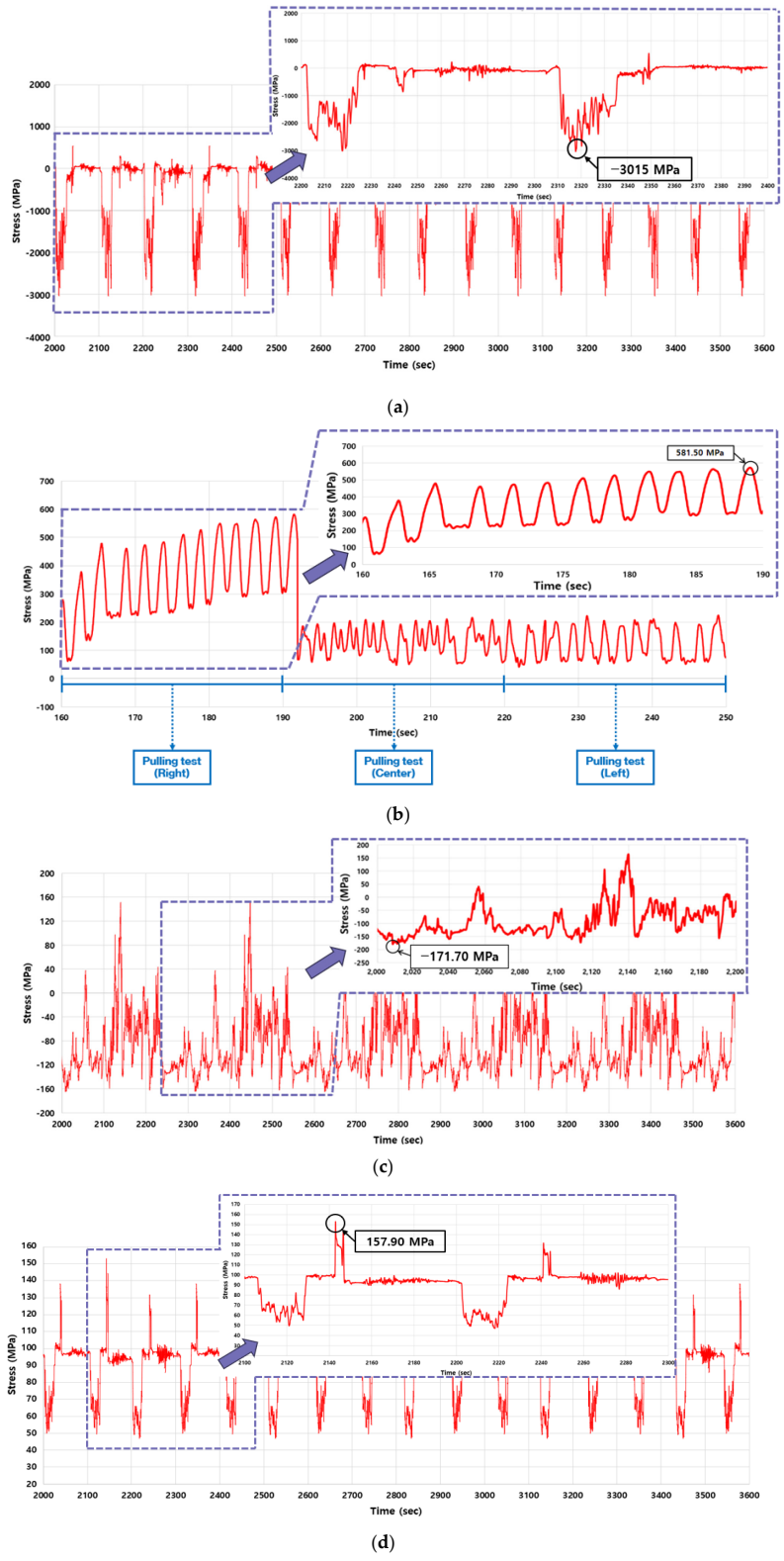

Figure 11. The location where the highest maximum stress occurred: (**a**) the 1st highest stress spot (G12, mount back side lower (R)); (**b**) the 2nd highest stress spot (G11, mount back side lower (L)); (**c**) the 3rd highest stress spot (G21, rear frame rear bottom (L)); (**d**) the 4th highest stress spot (G6, post bar).

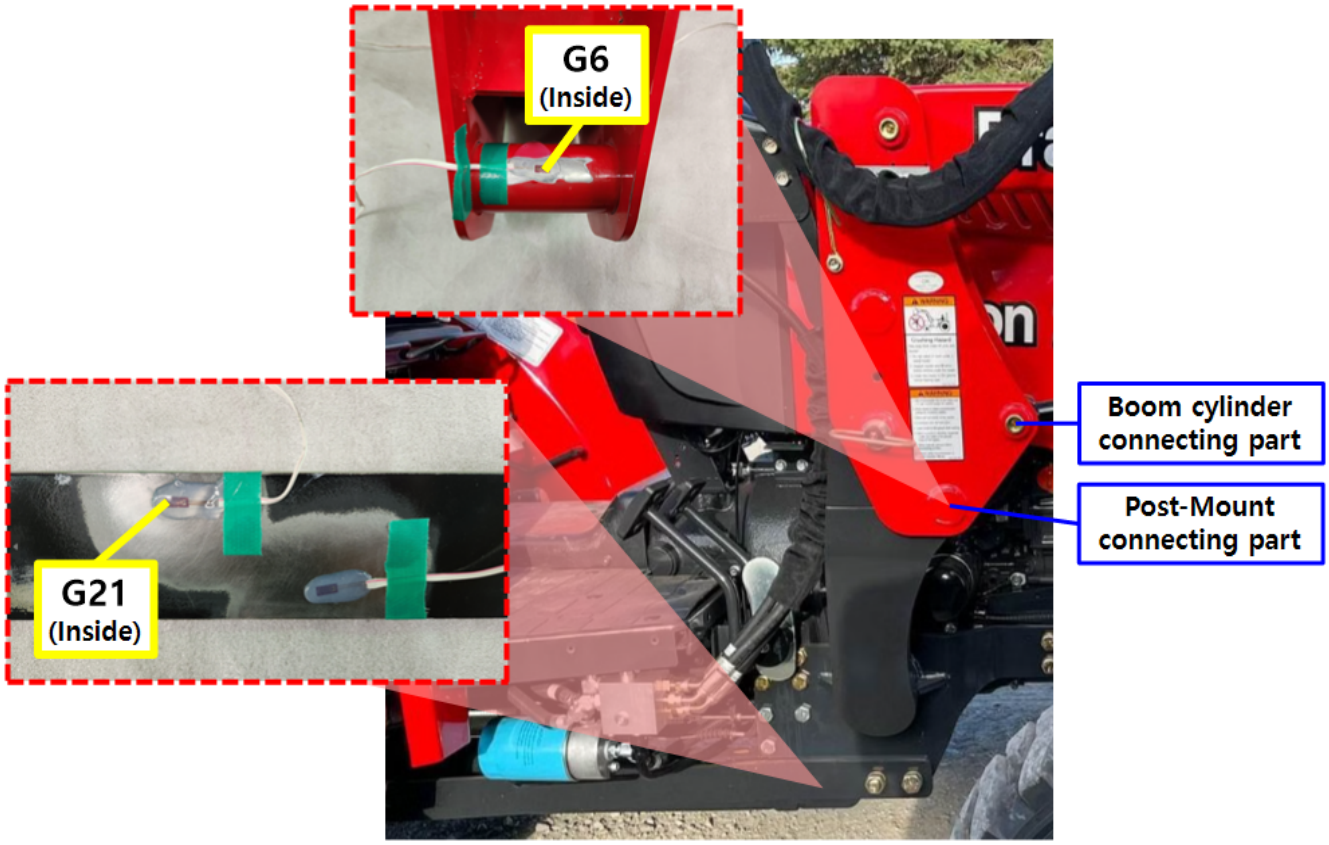

Figure 12. Measurement location of G6 and G21.

3.2. Safety Evaluation of the Front-End Loader

3.2.1. Static Safety Factor

The static safety factor at each location was obtained using the maximum stress measured during the total testing time and the yield strength of the front-end loader components (Table 9). The G11 and G12 locations of the mount had a static safety factor of less than 1.0 and the yielding of the material occurred because the maximum stress exceeded a yield strength of 331 MPa. At the other measurement locations, the static safety factor values ranged from 2.10 to 11.04 in the post, 3.11 to 9.38 in the mount, 1.93 to 11.47 in the rear frame, and 2.49 to 7.09 in the boom, indication that static yielding did not occur. These results indicate that it is necessary to modify the design of the mount, which primarily supports the weight and working load of the front-end loader. It is possible to increase the static safety factor by utilizing a material with a higher strength or by modifying the thickness or geometry to reduce the maximum stress level. In the case of the front-end loader used in this study, a material with a yield strength of 3015 MPa or higher must be used to apply a design modification method of increased strength. This is approximately nine times the yield strength of the material used, and considerable cost will be required to use such high-strength materials. Therefore, it is deemed proper to modify the design in the direction of mainly changing the thickness or geometry of the mount frame and using a material with a slightly higher strength as a complement.

Table 9. Static safety factor of each measurement location.

Component	Location	Static Safety Factor	Component	Location	Static Safety Factor
Post	G1	3.79	Rear frame	G18	9.09
	G2	4.86		G19	5.50
	G3	2.62		G20	8.80
	G4	2.85		G21	1.93
	G5	11.04		G22	2.55
	G6	2.10	Boom	G23	3.98
Mount	G7	9.38		G24	3.42
	G8	4.12		G25	3.46
	G9	4.87		G26	3.87
	G10	6.07		G27	7.09
	G11	0.57 (Static failure)		G28	6.97
	G12	0.10 (Static failure)		G29	2.49
	G13	3.58		G30	2.96
	G14	3.11		G31	4.09
Rear frame	G15	5.62		G32	6.17
	G16	8.54		G33	5.23
	G17	11.47		G34	7.18

3.2.2. Fatigue Life

The G11 and G12 locations of the mount were excluded from the fatigue life analysis due to the occurrence of static yielding. Table A1 (Appendix A) shows the damage sum and the damage ratio of each test condition at the measurement spots except for G11 and G12. At all measurement locations, the damage by the dumping test accounted for 72.5 to 99.9% of the total damage, showing that the dumping test is the condition that has the largest impact on fatigue damage. The damage that occurred in the pulling test represented 0 to 26.6% of the total damage. The sum of the damage that occurred in the drop, impact, and driving tests was less than 8% of the total damage, indicating that these three tests hardly affected fatigue damage. These results indicate that repeating the loading and unloading tasks using the bucket is the working condition that has the largest impact on fatigue damage among the tasks using the front-end loader.

The total damage sum at each measurement location ranged from 5.938×10^{-5} to 2.946×10^{-11}. Five measurement locations that exhibited the highest total damage were G21 of the rear frame, G3 of the post, G14 of the mount, G24 of the boom, and G23 of the boom, with values of 5.938×10^{-5}, 5.210×10^{-6}, 2.731×10^{-6}, 2.605×10^{-6}, and 1.868×10^{-6}, respectively. Table 10 shows the stress conditions that exhibited the largest impact on fatigue damage for the five locations. The number of cycles of the stress that caused the maximum damage was four to five, depending on the location, and this one stress condition represented 49.3 to 66.2% of the total damage.

At each measurement location, the fatigue life ranged from 1.919×10^5 to 1.394×10^9 h in the post, 3.661×10^5 to 7.312×10^8 h in the mount, 1.684×10^4 to 3.394×10^{10} h in the rear frame, and 3.839×10^5 to 2.461×10^7 h in the boom (Table 11). This satisfied the life span required by the front-end loader manufacturer. Therefore, it was concluded that fatigue life was satisfied at all measurement locations except for G11 and G12 of the mount where static yielding occurred. The five measurement locations that showed the shortest fatigue life were G21 of the rear frame (1.684×10^5 h), G3 of the post (1.919×10^5 h), G14 of the mount (3.661×10^5 h), G24 of the boom (3.839×10^5 h), and G23 of the boom (5.352×10^5 h). In the mount and rear frame, the fatigue life was also lowest at the spots where the highest maximum stress occurred among measurement locations. However, in the case of the post and boom, the spots with the highest maximum stress (G6 for the post and G29 for the boom) and those with the shortest fatigue life were different. This could be because the stress amplitude and the equivalent completely reversed stress were also high

at the spots with the higher maximum stress for the mount and rear frame, but they were relatively low at the spots with the highest maximum stress for the post and boom.

Table 10. Stress condition where higher damage occurred for five highest damage location.

Rank	Location	Mean Stress (MPa)	Stress Amplitude (MPa)	Equivalent Completely Reversed Stress (MPa)	Damage	Damage Ratio (%)	Number of Cycles
1	G21 (Rear frame rear bottom (L))	−6.89	157.94	155.67	3.93×10^{-5}	66.2	4
		−10.31	161.36	157.91	1.06×10^{-5}	17.9	1
		−1.14	98.43	98.20	2.94×10^{-6}	5.0	5
		−59.48	102.60	91.12	1.93×10^{-6}	3.3	5
		−60.91	98.13	86.91	1.48×10^{-6}	2.5	5
				Sum		94.9	
2	G3 (Post upper collar (R))	−15.68	52.46	50.77	3.30×10^{-6}	63.3	4
		−3.6	64.53	64.04	6.85×10^{-7}	13.2	1
				Sum		76.5	
3	G14 (Mount back side upper (L))	11.31	82.15	84.17	1.54×10^{-6}	56.4	5
		17.90	88.74	92.24	5.16×10^{-7}	18.9	1
		−11.28	58.70	57.33	1.78×10^{-7}	6.5	5
				Sum		81.8	
4	G24 (Front boom top side (R))	17.21	157.94	155.67	1.39×10^{-6}	53.7	5
		−10.31	161.36	157.91	7.38×10^{-7}	28.3	5
		−1.14	98.43	98.2	2.30×10^{-7}	8.8	5
		−59.48	102.6	91.12	1.87×10^{-8}	7.2	1
				Sum		98	
5	G23 (Front boom top side (L))	4.83	76.01	76.80	9.21×10^{-7}	49.3	4
		−3.41	67.69	67.21	3.48×10^{-7}	18.6	1
		−6.86	60.94	60.06	2.31×10^{-7}	12.4	5
		6.04	77.22	78.22	2.04×10^{-7}	10.9	5
		−1.75	66.04	65.80	7.72×10^{-8}	4.1	5
				Sum		95.3	

Table 11. Fatigue life for each measurement location.

Component	Location	Fatigue Life (hours)	Component	Location	Fatigue Life (hours)
Post	G1	6.447×10^5	Rear frame	G18	5.314×10^9
	G2	4.922×10^6		G19	1.675×10^9
	G3	1.919×10^5		G20	1.370×10^9
	G4	1.006×10^7		G21	1.684×10^4
	G5	1.394×10^9		G22	4.699×10^8
	G6	5.696×10^5	Boom	G23	5.352×10^5
Mount	G7	7.312×10^8		G24	3.839×10^5
	G8	2.962×10^8		G25	7.886×10^5
	G9	4.461×10^6		G26	6.585×10^5
	G10	5.714×10^6		G27	1.825×10^7
	G11	Static failure		G28	1.103×10^7
	G12	Static failure		G29	1.785×10^6
	G13	1.957×10^6		G30	9.943×10^5
	G14	3.661×10^5		G31	1.578×10^6
Rear frame	G15	1.225×10^8		G32	2.461×10^7
	G16	3.394×10^{10}		G33	8.922×10^6
	G17	3.025×10^9		G34	1.535×10^7

4. Conclusions

In this study, stress was measured for each component of an agricultural front-end loader to evaluate its structural safety. For that, we suggested new test code considering

actual operational environments of the front-end loader. They include five test conditions: drop test, impact test, pulling test, driving test, and dumping test. The drop test considers the load caused by the rise and fall of the bucket. The impact and pulling tests consider cases where an impact occurs due to an obstacle or when an excessive weight is applied to the bucket. The driving test considers the load caused by the irregular road surface while traveling, and the dumping test considers the operation of loading, transportation, and unloading of soil. A total of 1 h of testing was performed, considering the duty percentage for each test condition provided by the front-end loader manufacturer. Thirty-four stress measurement locations were determined as the stress concentration spots of the front-end loader components from a dynamic simulation.

As results, the pulling and dumping tests exhibited the highest stress among the test conditions. In this case, the maximum stress that exceeded the yield strength of the material occurred at some locations of the mount. This could be because the mount is an element that primarily supports various loads generated by the weight and working load of the front-end loader. Except for the locations of the mount where static yielding occurred, the static safety factor was 1.93 or higher at all measurement locations. The fatigue damage and fatigue life were calculated by applying the rain-flow counting, Goodman's equation, and Palmgren–Miner's linear cumulative damage rule to the measured time-series stress data. The stress conditions that cause fatigue damage were also identified. Most of the fatigue damage occurred in the dumping test, followed by the pulling test. The drop, impact, and driving tests negligibly affected fatigue damage. Fatigue life at all measurement locations, except for the locations of the mount where static yielding occurred, was within the range that satisfied the life span required by the front-end loader manufacturer. Therefore, the mount is structurally the weakest point of the front-end loader. A robust design for the mount is necessary to secure the structural integrity of the entire front-end loader.

Author Contributions: Conceptualization, formal analysis, methodology, validation, visualization, writing—original draft, J.-H.K.; Conceptualization, formal analysis, methodology, validation, visualization, writing—original draft, D.-H.G.; Conceptualization, formal analysis, funding acquisition, methodology, writing—review and editing, J.-S.N. All authors have read and agreed to the published version of the manuscript.

Funding: This work was partly supported by Korea Institute of Planning and Evaluation for Technology in Food, Agriculture and Forestry (IPET) through Machinery Mechanization Technology Development Program for Field Farming Program, grant funded by Ministry of Agriculture, Food and Rural Affairs (MAFRA) (RS-2023-00235957, 50) and Innovative Human Resource Development for Local Intellectualization program through the Institute of Information & Communications Technology Planning & Evaluation (IITP) grant funded by the Korea government (MSIT) (IITP-2024-RS-2023-00260267, 50).

Institutional Review Board Statement: Not applicable.

Data Availability Statement: Data is contained within the article.

Conflicts of Interest: The authors declare no conflict of interest.

Appendix A

Table A1. Total damage and damage ratio by test condition at each measurement location.

Location	Test Condition	Damage	Damage Ratio (%)	Total Damage	Location	Test Condition	Damage	Damage Ratio (%)	Total Damage
G1	Drop	5.752×10^{-12}	0.0	1.551×10^{-6}	G18	Drop	2.284×10^{-14}	0.0	1.882×10^{-10}
	Impact	2.862×10^{-10}	0.0			Impact	1.923×10^{-12}	1.0	
	Pulling	1.990×10^{-8}	12.8			Pulling	3.195×10^{-11}	17.0	
	Driving	8.161×10^{-10}	0.0			Driving	8.562×10^{-13}	0.5	
	Dumping	1.351×10^{-6}	87.2			Dumping	1.535×10^{-10}	81.5	
	Sum		100			Sum		100	
G2	Drop	5.767×10^{-12}	0.0	1.555×10^{-6}	G19	Drop	1.640×10^{-13}	0.0	5.969×10^{-10}
	Impact	2.870×10^{-10}	0.0			Impact	9.131×10^{-14}	0.0	
	Pulling	2.224×10^{-7}	14.3			Pulling	6.972×10^{-11}	11.7	
	Driving	8.183×10^{-10}	0.1			Driving	3.882×10^{-12}	0.7	
	Dumping	1.332×10^{-6}	85.6			Dumping	5.237×10^{-10}	87.6	
	Sum		100			Sum		100	
G3	Drop	7.234×10^{-9}	0.1	5.210×10^{-6}	G20	Drop	8.039×10^{-14}	0.0	7.300×10^{-10}
	Impact	2.870×10^{-10}	0.0			Impact	6.874×10^{-13}	0.1	
	Pulling	5.865×10^{-7}	11.3			Pulling	1.286×10^{-10}	17.6	
	Driving	4.122×10^{-7}	7.9			Driving	1.535×10^{-12}	0.2	
	Dumping	4.204×10^{-6}	80.7			Dumping	5.990×10^{-10}	82.1	
	Sum		100			Sum		100	
G4	Drop	3.224×10^{-12}	0.0	9.937×10^{-8}	G21	Drop	3.789×10^{-13}	0.0	5.938×10^{-5}
	Impact	1.781×10^{-9}	1.8			Impact	1.369×10^{-9}	0.1	
	Pulling	1.177×10^{-8}	11.9			Pulling	6.559×10^{-10}	0.0	
	Driving	2.490×10^{-11}	0.0			Driving	5.054×10^{-10}	0.0	
	Dumping	8.579×10^{-8}	86.3			Dumping	5.937×10^{-5}	99.9	
	Sum		100			Sum		100	
G5	Drop	6.125×10^{-12}	0.9	7.173×10^{-10}	G22	Drop	8.048×10^{-13}	0.0	2.128×10^{-9}
	Impact	4.683×10^{-14}	0.0			Impact	2.430×10^{-13}	0.0	
	Pulling	9.700×10^{-11}	13.5			Pulling	2.661×10^{-10}	12.4	
	Driving	3.070×10^{-12}	0.4			Driving	2.549×10^{-11}	1.2	
	Dumping	6.111×10^{-10}	85.2			Dumping	1.855×10^{-9}	86.4	
	Sum		100			Sum		100	

Table A1. *Cont.*

Location	Test Condition	Damage	Damage Ratio (%)	Total Damage	Location	Test Condition	Damage	Damage Ratio (%)	Total Damage
G6	Drop	1.654×10^{-9}	0.1	1.756×10^{-6}	G23	Drop	1.246×10^{-11}	0.0	1.868×10^{-6}
	Impact	1.661×10^{-9}	0.1			Impact	9.269×10^{-9}	0.5	
	Pulling	1.876×10^{-7}	10.7			Pulling	1.874×10^{-7}	10.0	
	Driving	6.932×10^{-8}	3.9			Driving	1.282×10^{-9}	0.1	
	Dumping	1.496×10^{-6}	85.2			Dumping	1.670×10^{-6}	89.4	
	Sum		100			Sum		100	
G7	Drop	1.137×10^{-13}	0.0	1.368×10^{-9}	G24	Drop	1.332×10^{-11}	0.0	2.605×10^{-6}
	Impact	8.327×10^{-11}	6.2			Impact	4.427×10^{-9}	0.2	
	Pulling	2.804×10^{-10}	20.5			Pulling	4.540×10^{-7}	17.4	
	Driving	3.376×10^{-12}	0.2			Driving	2.168×10^{-9}	0.1	
	Dumping	9.995×10^{-10}	73.1			Dumping	2.144×10^{-6}	82.3	
	Sum		100			Sum		100	
G8	Drop	7.747×10^{-13}	0.0	3.376×10^{-9}	G25	Drop	1.225×10^{-11}	0.0	1.268×10^{-6}
	Impact	1.001×10^{-12}	0.0			Impact	6.826×10^{-9}	0.5	
	Pulling	8.982×10^{-10}	26.6			Pulling	1.955×10^{-7}	15.5	
	Driving	2.898×10^{-11}	0.9			Driving	1.211×10^{-9}	0.1	
	Dumping	2.447×10^{-9}	72.5			Dumping	1.064×10^{-6}	83.9	
	Sum		100			Sum		100	
G9	Drop	6.745×10^{-11}	0.0	2.241×10^{-7}	G26	Drop	8.734×10^{-12}	0.0	1.519×10^{-6}
	Impact	4.773×10^{-9}	2.1			Impact	3.989×10^{-9}	0.3	
	Pulling	3.125×10^{-8}	13.9			Pulling	2.188×10^{-7}	14.6	
	Driving	4.052×10^{-9}	1.8			Driving	1.903×10^{-9}	0.1	
	Dumping	1.842×10^{-7}	82.2			Dumping	1.272×10^{-6}	85.0	
	Sum		100			Sum		100	
G10	Drop	3.495×10^{-11}	0.0	1.750×10^{-7}	G27	Drop	8.392×10^{-13}	0.0	5.479×10^{-8}
	Impact	4.502×10^{-11}	0.0			Impact	1.769×10^{-10}	0.3	
	Pulling	2.113×10^{-8}	12.2			Pulling	8.085×10^{-9}	14.3	
	Driving	5.800×10^{-10}	0.3			Driving	4.468×10^{-11}	0.1	
	Dumping	1.528×10^{-7}	87.5			Dumping	4.826×10^{-8}	85.3	
	Sum		100			Sum		100	

Table A1. *Cont.*

Location	Test Condition	Damage	Damage Ratio (%)	Total Damage	Location	Test Condition	Damage	Damage Ratio (%)	Total Damage
G11	Static failure				G28	Drop	3.215×10^{-13}	0.0	9.064×10^{-8}
						Impact	9.897×10^{-11}	0.1	
						Pulling	4.989×10^{-9}	5.5	
						Driving	4.128×10^{-11}	0.0	
						Dumping	8.495×10^{-8}	94.4	
						Sum		100	
G12	Static failure				G29	Drop	1.656×10^{-13}	0.0	5.602×10^{-7}
						Impact	7.123×10^{-9}	1.2	
						Pulling	4.274×10^{-8}	7.5	
						Driving	7.500×10^{-11}	0.0	
						Dumping	5.242×10^{-7}	91.3	
						Sum		100	
G13	Drop	3.545×10^{-10}	0.1	5.110×10^{-7}	G30	Drop	7.385×10^{-14}	0.0	1.006×10^{-6}
	Impact	7.731×10^{-10}	0.2			Impact	2.067×10^{-9}	0.1	
	Pulling	8.645×10^{-8}	16.8			Pulling	8.669×10^{-8}	8.2	
	Driving	1.260×10^{-8}	2.5			Driving	5.701×10^{-11}	0.0	
	Dumping	4.108×10^{-7}	80.4			Dumping	9.797×10^{-7}	91.7	
	Sum		100			Sum		100	
G14	Drop	1.116×10^{-9}	0.0	2.731×10^{-6}	G31	Drop	1.175×10^{-14}	0.0	6.337×10^{-7}
	Impact	1.440×10^{-10}	0.0			Impact	2.046×10^{-10}	0.0	
	Pulling	3.285×10^{-7}	11.9			Pulling	5.167×10^{-8}	8.5	
	Driving	1.509×10^{-7}	5.5			Driving	7.456×10^{-13}	0.0	
	Dumping	2.287×10^{-6}	82.6			Dumping	5.571×10^{-7}	91.5	
	Sum		100			Sum		100	
G15	Drop	1.011×10^{-15}	0.0	8.164×10^{-9}	G32	Drop	3.554×10^{-14}	0.0	4.063×10^{-8}
	Impact	1.054×10^{-10}	1.3			Impact	2.448×10^{-11}	0.1	
	Pulling	7.194×10^{-10}	8.8			Pulling	2.431×10^{-9}	9.0	
	Driving	3.432×10^{-11}	0.4			Driving	3.220×10^{-12}	0.0	
	Dumping	7.305×10^{-9}	89.5			Dumping	2.443×10^{-8}	90.9	
	Sum		100			Sum		100	

Table A1. *Cont.*

Location	Test Condition	Damage	Damage Ratio (%)	Total Damage	Location	Test Condition	Damage	Damage Ratio (%)	Total Damage
G16	Drop	1.341×10^{-14}	0.0	2.946×10^{-11}	G33	Drop	3.532×10^{-14}	0.0	1.121×10^{-7}
	Impact	8.758×10^{-14}	0.3			Impact	1.949×10^{-9}	1.8	
	Pulling	5.027×10^{-12}	17.1			Pulling	5.268×10^{-10}	0.5	
	Driving	5.180×10^{-13}	1.8			Driving	2.800×10^{-12}	0.0	
	Dumping	2.379×10^{-11}	80.8			Dumping	1.073×10^{-7}	97.7	
	Sum		100			Sum		100	
G17	Drop	4.663×10^{-14}	0.0	3.306×10^{-10}	G34	Drop	2.493×10^{-14}	0.0	6.516×10^{-8}
	Impact	1.518×10^{-13}	0.1			Impact	6.084×10^{-10}	1.0	
	Pulling	4.029×10^{-11}	13.3			Pulling	4.915×10^{-10}	0.8	
	Driving	2.021×10^{-12}	0.7			Driving	4.588×10^{-12}	0.0	
	Dumping	2.601×10^{-10}	85.9			Dumping	6.169×10^{-8}	98.2	
	Sum		100			Sum		100	

References

1. Glancey, J.; Upadhyaya, S.; Chancellor, W.; Rumsey, J. Prediction of Agricultural Implement Draft using an Instrumented Analog Tillage Tool. *Soil Tillage Res.* **1996**, *37*, 47–65. [CrossRef]
2. Lee, C.J.; Ha, J.W.; Choi, D.S.; Kim, H.J. Development of a Self-leveling System for the Bucket of an Agricultural Front-end Loader Using an Electro Hydraulic Proportional Valve and a Tilt Sensor. *J. Drive Control* **2015**, *12*, 60–70. [CrossRef]
3. Kim, S.J.; Gim, D.H.; Jang, M.K.; Hwang, S.J.; Kim, J.H.; Yang, Y.J.; Nam, J.S. Development of Regression Model for Predicting the Maximum Static Friction Force of Tractors with a Front-End Loader. *J. Biosyst. Eng.* **2023**, *48*, 329–338. [CrossRef]
4. Jaiswal, S.; Korkealaakso, P.; Åman, R.; Sopanen, J.; Mikkola, A. Deformable Terrain Model for the Real-Time Multibody Simulation of a Tractor with a Hydraulically Driven Front-Loader. *IEEE Access* **2019**, *7*, 172694–172708. [CrossRef]
5. Han, G.H.; Kim, K.D.; Ahn, D.V.; Park, Y.J. Comparative Analysis of Tractor Ride Vibration According to Suspension System Configuration. *J. Biosyst. Eng.* **2023**, *48*, 69–78. [CrossRef]
6. Nasarwanji, M.; Pollard, J.; Porter, W. An Analysis of Injuries to Front-end Loader Operators during Ingress and Egress. *Int. J. Ind. Ergon.* **2018**, *65*, 84–92. [CrossRef]
7. Modak, S.; Raheman, H. Effects of Various Machine Parameters on Cutting Performance for High-speed Cutting of Paddy Crop. *J. Biosyst. Eng.* **2022**, *47*, 181–196. [CrossRef]
8. Bhola, M.; Kumar, A.; Kumar, N. Energy-efficient Control of Hydrostatic Transmission of a Front-end Loader Machine Using Machine Learning Algorithm and its Sensitivity Analysis. *Proc. Inst. Mech. Eng. Part D J. Automobile. Eng.* **2022**, *13*, 237. [CrossRef]
9. Lim, G.S.; Lee, B.Y. Study on the Impact Analysis of Front Loader for Tractor. *J. Korean Soc. Manuf. Technol.* **2015**, *16*, 5051–5059. [CrossRef]
10. Cho, B.J.; Ahn, S.W.; Lee, C.J.; Yoon, Y.H.; Lee, S.S.; Kim, H.J. Improved Design of Hydraulic Circuit of Front-end Loader for Bump Shock Reduction of an Agricultural Tractor. *J. Drive Control* **2016**, *13*, 10–18. [CrossRef]
11. Ahn, S.W.; Kim, H.J.; Lee, S.S.; Choi, D.S. Study on Driving Shock Reduction of a Front End Loader by Accumulator. *Proc. KSAM* **2014**, *19*, 91–92.
12. Latoree, J.I.; Arana, I.; Ballesteros, T.; Pintor, J.M.; Alfaro, J.R. Front End Loader with Automatic Levelling for Farm Tractors. *Biosyst. Eng.* **2016**, *148*, 111–126. [CrossRef]
13. Kwon, G.B.; Shin, D.Y. Optimum Design of Mini Loader Based on the Design of Experiment. *Trans. Korean Soc. Mech. Eng. A* **2011**, *35*, 693–699. [CrossRef]
14. Hensh, S.; Tewari, V.K.; Upadhyay, G. An instrumentation system to measure the loads acting on the tractor PTO bearing during rotary tollage. *J. Terramech.* **2021**, *96*, 1–10. [CrossRef]
15. Malon, H.; Ayuda, A.; Garcia, F.; Vidal, M.; Cuartero, J. Application of Low-Cost Sensors for the Development of a Methodology to Design Front-End Loaders for Tractors. *J. Sens.* **2020**, *2020*, 1–13. [CrossRef]
16. Park, Y.J.; Shim, S.B.; Nam, J.S. Experimental Study on the Structural Safety of the Tractor Front-End Loader against Impact Load. *J. Biosyst. Eng.* **2016**, *41*, 153–160. [CrossRef]
17. Yilmaz, D.; Hamamci, E.; Salik, D.; Ahiskali, Y. Structural Analysis of Agricultural Machinery: A Case Study for a Transport Chassis of a Spraying Machine. *J. Agric. Mach. Sci.* **2011**, *7*, 405–409.
18. Budynas, R.G.; Nisbett, J.K. *Shigley's Mechanical Engineering Design*, 9th ed.; Mcgraw-Hill: New York, NY, USA, 2011; pp. 427–436.
19. Mourad, A.; Alomomani, A.; Seikh, I.; Elsheikh, A. Failure Analysis of Gas and Wind Turbine Blades: A review, Eng. *Fail. Anal.* **2023**, *146*, 107107. [CrossRef]
20. Lee, G.H.; Moon, B.E.; Basak, J.; Kim, N.E.; Paudel, B.; Jeon, S.W.; Kook, J.H.; Kang, M.Y.; Ko, H.J.; Kim, T.H. Assessment of Load on Threshing Bar During Soybean Pod Threshing. *J. Biosyst. Eng.* **2023**, *48*, 478–486. [CrossRef]
21. Eldogan, Y.; Cigeroglu, E. Vibration Fatigue Analysis of a Cantilever Beam Using Different Fatigue Theories. In *Topics in Modal Analysis, Volume 7: Proceedings of the 31st IMAC, A Conference on Structural Dynamics*; Springer: New York, NY, USA, 2013; Volume 7, pp. 471–478. [CrossRef]
22. Lee, W.S.; Lee, H.W. A Study on the Prediction of the Fatigue Life of a Lug through the Finite Element Analysis. *J. Korean Soc. Precis. Eng.* **1998**, *15*, 88–95.

Disclaimer/Publisher's Note: The statements, opinions and data contained in all publications are solely those of the individual author(s) and contributor(s) and not of MDPI and/or the editor(s). MDPI and/or the editor(s) disclaim responsibility for any injury to people or property resulting from any ideas, methods, instructions or products referred to in the content.